4-19-2018

Brain Connectivity Analysis of Normal Hearing and Hearing Impaired Participants Based on the Cortical Surface EEG Data

MD Sultan Mahmud

BRAIN CONNECTIVITY ANALYSIS OF NORMAL HEARING AND HEARING IMPAIRED PARTICIPANTS BASED ON THE CORTICAL SURFACE EEG DATA

by

Md Sultan Mahmud

A Thesis

Submitted in Partial Fulfillment of the

Requirements for the degree of

Master of Science

Major: Electrical and Computer Engineering

The University of Memphis

May 2018

Dedicated to My Parents, Wife, Brothers, and Advisor

ACKNOWLEDGMENTS

First of all, I would like to express my sincere gratitude to my advisor Prof. Dr. Mohammed Yeasin for giving me an opportunity in his lab to conduct research work during my graduate studies. I would like to thank him for his continuous mentoring, support, and guidance throughout the work. I could not have imagined having a better advisor and mentor for my MS degree. I would also like to thank my thesis committee members Dr. Gavin M. Bidelman and Dr. Madhusudhanan Balasubramanian for their encouragement, and insightful comments. Again special thanks to Dr. Bidelman for giving data and research guideline in the point of views of neuroscience.

This study would not be accomplished without the research assistantship from my advisor. I also thank the Claude Alain's research group at Rotman Research Institute in Toronto, Canada, and the thirty-two participants for their time.

I thank my fellow lab mates Faruk Ahmed and Rakib Al-Fahad for all the discussions we had related to the research and for lending their hands when needed the most.

Last but not least, I would like to thank my parents, wife, and brothers for the sacrifices they made without which this work would not have been possible.

ABSTRACT

Hearing is an important sensory function of human communication and alerts people of dangerous conditions by detecting the emergency auditory alarm, sirens. We localized the source of EEG data (Hearing EEG data) into the cortical surface by solving the inverse problem and extracted the time series data from the 68 regions of Deskin-Killiany (DK) atlas. By using Granger Causality and Phase Transfer Entropy, we analyzed the brain connectivity of people experiencing normal hearing (NH) and hearing loss (HL). These results showed that NH and HL listeners' connectivity levels are not the same. Moreover, we investigated which connectivities of the human brain are changed after hearing loss. We also performed a statistical analysis between eight regions of the brain; those are associated with the auditory and language processing tasks and significant changes were found in the primary Auditory and Broca's areas. It is noticeable that HL listeners utilize the top-down modulation to perceive the sounds. Finally, we also found that neural and behavioral results are correlated.

TABLE OF CONTENTS

LIST OF FIGURES

1. INTRODUCTION

Here we will discuss hearing loss difficulties, how the human brain is activated by a stimulus, auditory and language processing, goals and objectives of this work.

1.1. PROBLEM DESCRIPTION

Hearing is an essential sensory function that allows humans to communicate properly and to be aware of dangers such as emergency alerts, e.g., sirens and alarms. Hearing loss is associated with cognitive decline, social isolation, and loneliness in older adults. When the auditory perception is difficult, greater cognitive resources are engaged in auditory perception processing [1]. Most listening has some background noise, and typically older adults have difficulty in detecting speech sounds [2]. According to the National Health and Nutrition Examination Survey (NHANES), hearing impairment increases dramatically with age [3]. Hearing loss is one of the key contributors to the growing problem of disability in the United States [4]. Regions of the human brain are interconnected and activated based on the stimulus. Human and other vertebrates' temporal lobes process the auditory information. For instance, during the information processing Auditory, Broca's and Motor areas are activated. They are connected and responsible for hearing loss. We will identify the significant changes of functionality in the Auditory, Broca's and Motor areas. Different neuroimaging modalities (fMRI, EEG, MEG, etc.) are used for connectivity analysis [5]. For this study, we used Electroencephalography (EEG). It is more famous for clinical, investigating the brain functionality and mental processing due to high temporal resolution and non-invasive technology [6], [7].

1.2. THE GOALS AND OBJECTIVES OF THIS WORK

The primary goal of this interdisciplinary research is to apply robust connectivity analysis approaches that can provide better and significant results in identifying the neural effects of hearing loss.

The goals are as follows:

i) To localize the source of EEG on the cortical surface,

ii) To extract the time series data from the cortical surface,

iii) To find the whole brain connectivity by using different robust methods,

iv) To find the significant ROIs those are associated with the auditory and speech processing task, and

v) To investigate the relationship between the behavioral and neural results.

The objectives of this thesis are as follows:

a) We will consider a forward model that can compute the head model. Here we will use the Boundary Element Model (BEM) because it is popular and robust.

b) We will consider a mathematical model that can solve the inverse problem. We will consider a widely used method standard low-resolution brain electromagnetic tomography (sLORETA).

c) We will measure the whole brain connectivity through Phase Transfer Entropy (PTE) and Granger Causality (GC) based on the cortical surface time series data.

d) We will also perform a statistical analysis of two cohorts and different conditions in the Auditory, Broca's and Motor areas based on the PTE and GC measured strength.

e) We will compare the PTE and GC results.

f) Finally, we will investigate the neural and behavioral correlation.

The rest of the thesis is organized as follows: chapter 2 describes the recent related works serving as the background of this work; chapter 3 discusses the participant details, stimulus, EEG recording, preprocessing, source localization and behavioral results; chapter 4 discusses the results in a circular graph and statistical analysis; and finally, chapter 5 concludes the thesis.

2. RELATED WORKS

Here we will discuss recent related works on human brain connectivity, EEG source localization, connectivity analysis techniques, top-down and bottom-up modulation.

Our brain is highly complex. It has multiple regions those are engaged based on the different tasks. The brain coordinates multiple regions' functionality based on the stimulus. Some of the brain regions are structurally connected, and some of them are functionally connected. There are three types of brain connectivity. Anatomical, functional and effective connectivity [8]. The anatomical connection represents the connection between the regions of the white matter tracts. On the other hand, the functional connectivity corresponds to the magnitude of the time series correlation in activity and may occur between the anatomical and unconnected regions [8]. The effective connectivity is the union of structural and functional connectivity that describes the flow of information [9].

Source Localization. Based on the stimulus different brain regions are activated. The neurons are firing inside the brain, but EEG is measured on the scalp surface of the head. Source localization is important in clinical interpretations and a better understanding of functional abnormalities and behavioral research. Over the last couples of decades, there is a significant progress in source localization.

There are a few essential components for successful source localization: (i) an electrical forward head model, (ii) an individual source space model, and (iii) an inverse source localization model [10] . The process of prediction the scalp surface potentials from the emerging electric current that generated by plenty of neurons firing inside the brain is called the EEG forward model. The forward model is a head model to estimate the potential of the scalp. There are different head models (e.g., spherical and non-spherical) used for source localization.

The spherical boundary element method (BEM) head model is widely used. This head model is based on the Montreal Neurological Institute (MNI) template head image. The BEM is composed of two-dimensional triangulated mesh layers (boundaries). There are four layers considered (scalp, skull, CSF, and cortex). The different compartments have different conductivity values, but within each compartment the conductivity assumes to be the isotropic and homogenous [11], [12]. The EEG source localization depends on a few factors such as sufficient sampling, accurate head model and the approximation of the volume conduction and well-known inverse problem [13], [14].

On the other hand, the process of predicting the locations of sources of neurons from the scalp surface measured EEG potential is referred to as an inverse problem. The aim of the inverse problem is reconstructing the brain electrical activity on the cortex from the scalp surface EEG measurements. Most of the EEG source localization techniques consider the homogenous head model that represents the physical properties of the human head volume conductor. In distributed models, the location and orientation of a large number of dipoles are fixed over the cortical surface. In this case, the amplitude calculation of a number of dipoles sample is required at every time point in a fixed grid [15]. sLORETA is a distributed inverse method that used with a BEM forward model. The constraint modeling of sLORETA is based on the neighbor neuronal populations are more likely than the non-neighbored neuronal populations undergoes synchronous depolarization or evoked response. However, the sLORETA gives a smoothed solution because of neighborhood sources are conditioned to assume the similar strength [12].

The electric activity at the scalp surface can be represented by the following equation:

$$f = L.q$$

Where f is the simulated measurement electric potential vector, L is the lead field matrix, and q is the dipole column vector that contains the location and strength information of the source. The accuracy of the source localization is measured by comparing the estimated source and simulated measured. The best fitting of the dipole can be calculated by minimizing the error between the simulated value and forward computed value.

$$Error = |R - L.q|^2$$

where R is the simulated computed value.

Connectivity analysis methods. Different methods are using for functional connectivity analysis: correlation, coherence, Granger Causality (GC), Phase Transfer Entropy (PTE), Phase Locking Value (PLV), Phase Slope Index (PSI) [16], [17]. Functional connectivity describes the statistical differences between two or more variables, the dependencies can be undirected (correlation, coherence) or directed (GC, PTE) [18]. The GC and coherence are based on a rigorous statistical theory of stochastic processes. The linear measure such as coherence or PLV will capture this interaction. Cross-frequency coupling is nonlinear. GC and PTE describe the directed influences of two signals.

Out of the above mentioned methods, three methods are using for competitive connectivity analysis. GC, dynamic causal modeling, and PTE. PTE quantifies the entropy between the phase time series. PTE is a robust and efficient method. It works on noise conditions [19]. GC is implemented in time or frequency domain based on the autoregressive modeling of the signals and their interactions. GC is ill-suited to whole brain network analysis [20]. On the spectra analysis, GC could not find phase information. Transfer entropy is model-free, there is no assumption on signal or interaction structure. PTE is a good candidate for the phase-based connectivity. The details of the mathematical elaboration of PTE and GC is given in [19], [18].

Top-down and bottom-up modulation. The human auditory system is composed of a set of complicated connections. The sound information from the cochlea to auditory system passes through the ascending pathways. Perception of the external sounds entails with the detection of bits and pieces of partially degraded external sound sources [21]. Moreover, speech perception also involves the top-down and bottom-up process. The top-down process relies on prior knowledge (e.g., language experience) and bottom-up process depends on the instant auditory input (e.g., incoming data, data-driven). The bottom-up process occurs for the first 200 ms for pitch perception, and the top-down process happens in a late time window around 300-500 ms [22]. LH has the advantage of top-down processing. It helps the listeners to understand the meaning and context of speech or sentence. Aging affects peripheral hearing and changes central auditory processing. Several studies found that the older adults with hearing loss exploit the top-down process for perceiving the corrupted or ambiguous sounds. These studies showed a few effects. For instance, when processing the non-ambiguous sounds, aging is associated with the disrupting central auditory processing that cannot reduce the signal to noise ratio of the input signal. The top-down modulation is engaged to enhance the speech perception, and sensitivity to the change of input coming from the peripheral auditory apparatus may provide plastic effects after hearing loss [21], [19].

3. METHODS

We are reanalyzing the preexisting data that was originally collected by the Claude Alain's group at Rotman Research Institute in Toronto, Canada [23]. We will analyze the brain connectivity of NH and HL based on this data. Details of the dataset and methodology will be described in this section. In this section, we will discuss participants' details, stimuli and task, EEG recording, source localization process, behavioral results, and brain atlas that we will use for this study.

3.1. PARTICIPANTS AND STIMULUS

"Thirty-two older adults (13 normal hearing and 19 hearing impaired) were recruited from the greater Toronto Area in our ongoing research on aging and auditory system. The age of the participants between 52 to 72 years. None of them reported a history of neurological or psychiatric diseases. A puretone audiometry was conducted at octave frequencies 250 to 8000 Hz, based on the listeners' thresholds, the cohort was divided into normal hearing and hearing loss groups (Figure 3.2 A). Normal-hearing (NH) listeners were classified as those having the average hearing threshold (250-8000 Hz) better than the 25 dB HL across both ears. On the other hand, those having average hearing thresholds poorer than the 25 dB HL were classified as hearing loss (HL). This separation resulted in pure-tone averages (PTAs) (i.e., mean of 500, 1000, 2000 Hz) that were ~10 dB better in NH compared to HL listeners (NH: 15.3±3.27 dB HL, HL: 26.4±7.1 dB HL; $t_{2.71}$=-5.95, p<0.0001). Importantly, the groups were otherwise matched in age (NH: 66.2±6.1 years, HL: 70.4±4.9 years; $t_{2.22}$ = -2.05, p = 0.052) and gender balance (NH: 5/8 male/female; HL: 11/8; Fisher's exact test, p = 0.47). Age and hearing loss were not correlated in our sample (Pearson's r = 0.29, p = 0.10). Participants were compensated for their

time and gave written informed consent in compliance with a protocol approved by the Baycrest Centre research ethics committee [23]".

We prepared three consonant-vowel (CV) tokens (/ba/, /pa/, /ta/).The stimuli presentation scenario is depicted in Figure 3.1. A total of 6210 CVs were presented in both clean and noise-degraded conditions (each spread over three blocks). The stimulus set included a total of 3000 /ba/, 3000/pa/, and 210 /ta/ tokens (spread evenly over three blocks).

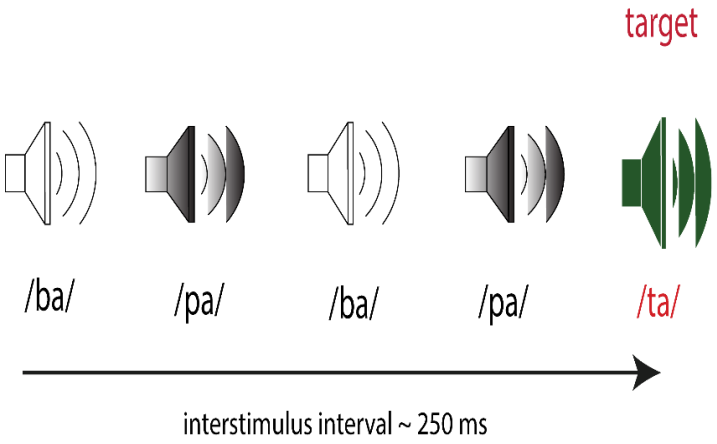

Figure 3.1 Auditory stimuli presentation

"Each token was 100 ms in duration. For each block, speech tokens were presented back-to-back in random order with a rapid interstimulus interval (~250 ms) [24]. In a pseudo-random schedule frequent (/ba/, /pa/) and infrequent (/ta/) tokens were presented and also maintain that at least two frequency stimuli intervened between target /ta/ tokens. Listeners were instructed to respond each time they detected the target token (/ta/) via a button press on the computer. Reaction time (RT) and detection accuracy (%) were logged. These same procedures were then repeated using an identical speech triplet but presented in four talker noise babble at 10 dB SNR [25].The babble was presented continuously so that it was not time-locked to the stimulus, providing a constant backdrop of interference in the noise condition [26], [27]. Comparisons

between behavioral performance between clean and degraded stimuli allowed us to assess the impact of acoustic noise and differences between normal and hearing-impaired listeners on speech perception. Importantly, this task ensured that ERPs were recorded online, during active speech perception [28].

Stimulus presentation was controlled by a MATLAB routed to a TDT RP2 interface (Tucker-Davis Technologies) and delivered binaurally at an intensity of 82 dB SPL through insert earphones (ER-2; Etymotic Research) [23]."

3.2. BEHAVIORAL RESULTS

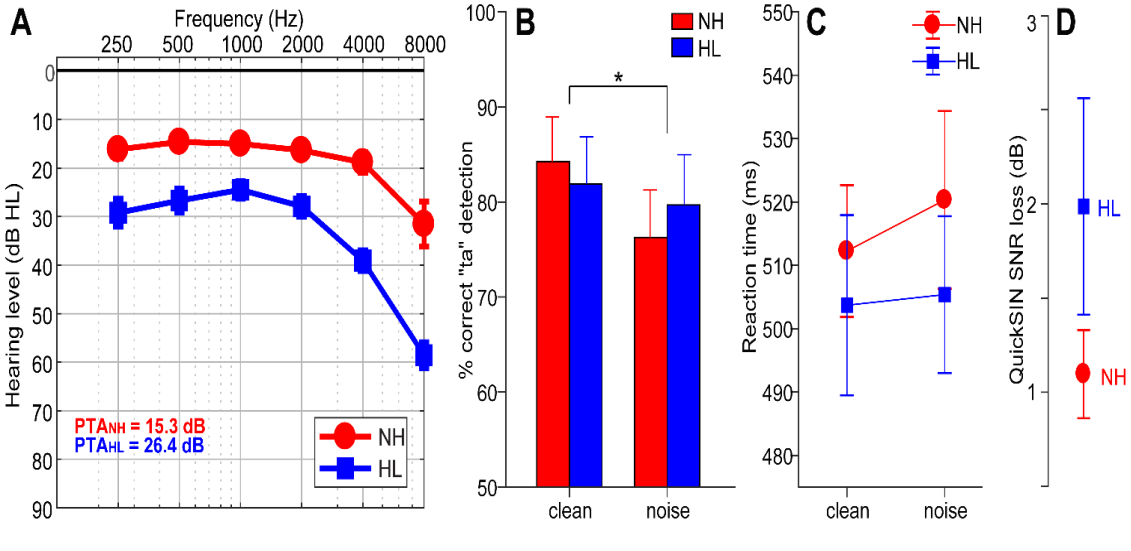

Figure 3.2 Behavioral Results [23]

"Behavioral accuracy and reaction time for target speech detection is shown for each group and noise condition in Figure 3.2. An ANOVA revealed a main effect of SNR on perceptual accuracy, which was lower for noise-degraded compared to clean speech [F1, 30 = 5.66, p = 0.024; Figure 3.2 B]. However, groups differed neither in their accuracy [F1, 30 = 0.01, p = 0.94] nor speed [F1, 30 = 0.47, p = 0.49; Figure 3.2 C] of speech detection. Behavioral QuickSIN scores are shown for NH and HL listeners in Figure 3.2D. On average, HL individuals achieved

performance within ~1 dB of NH listeners, and QuickSIN scores did not differ between groups [t2.35= -1.43, p = 0.16]. Nevertheless, HL listeners did show more variability in SIN performance compared to NH listeners [F-test for equal variances: F12, 18 = 0.11, p = 0.0004]. Collectively, these results suggest that hearing loss in the cohort was not yet egregious enough to yield measurable deficits in speech perception [23]".

3.3. ELECTROPHYSIOLOGICAL RECORDINGS AND ANALYSIS

"EEG acquisition and preprocessing. The neural activity was recorded from the scalp surface by 32 channels at standard 10-20 locations during the behavioral task detection [29]. Recording EEGs during the active listening task allowed us to control for attention and assess the relative influence of brainstem and cortex during online speech perception. EEGs were digitized at a sampling rate of 20 kHz using SynAmps RT amplifiers (Compumedics Neuroscan). Electrodes placed along the zygomatic arch (FT9/10) and the outer canthi and superior/inferior orbit of the eye (IO1/2, LO1/2) monitored ocular activity and blinked artifacts. During online acquisition, all electrodes were referenced to the Cz electrode. This channel was reinstated, and data were re-referenced off-line to a common average reference for subsequent analyses. Electrode impedances were maintained ≤ 5 kΩ through the duration of testing.

Subsequent pre-processing was performed in BESA® Research v6.1 (BESA, GmbH). Ocular artifacts (saccades and blinks) were first corrected in the continuous EEG using a principal component analysis (PCA) [30] EEGs were then epoched into single trials (-10-200 ms) per condition and baseline-corrected to the pre-stimulus period [23]."

Source localization method. After the above preprocessing, we averaged all the trials by conditions (clean and noise), individual and cohorts (NH and HL) and filtered (1-40 Hz). First of all, we have considered a more realistic forward model, e.g., Boundary Element Model (BEM) that required for source localization. The BEM is composed of two dimensional triangulated

mesh layers (boundaries). There are four layers considered (scalp, skull, CSF, and cortex). The different compartments have different conductivity values but within each compartment the conductivity is assumed to be isotropic and homogenous. The noise covariance matrix was measured from the pre-stimulus recording data. sLORETA is a distributed inverse method that was used with a BEM forward model. The default setting parameters of sLORETA in brainstorm are: noise covariance regularization parameters (regularize noise covariance 0.1), regularization parameters $1/\lambda$ (SNR 3.00) [31]. In this work, we used a low-resolution cortical surface with 1500 vertices and assigned a diploe in every vertex, and their orientation is perpendicular to the cortical surface. The constraint modeling of sLORETA is based on the assumption that neighbor neuronal populations are more likely than non-neighbored neuronal populations to undergo synchronous depolarization or evoked response. Moreover, sLORETA gives a smoothed solution because of neighborhood sources are conditioned to assume the similar strength [12]. Once we have solved the inverse problem, the cortical surface data can be visualized in different atlases. The source localization processing by Brainstorm tools is shown in Figure 3.3.

For this study, we have considered a widely used brain parcellation scheme called Desikan-Killinay (DK) atlas. It has 34 cortical regions of interest (ROIs) in each hemisphere [32], [33]. The DK atlas is presented in Figure 3.4. The time series data were extracted from the 68 ROIs. The full and shortened names of DK brain ROIs are shown in in Table-3.1:

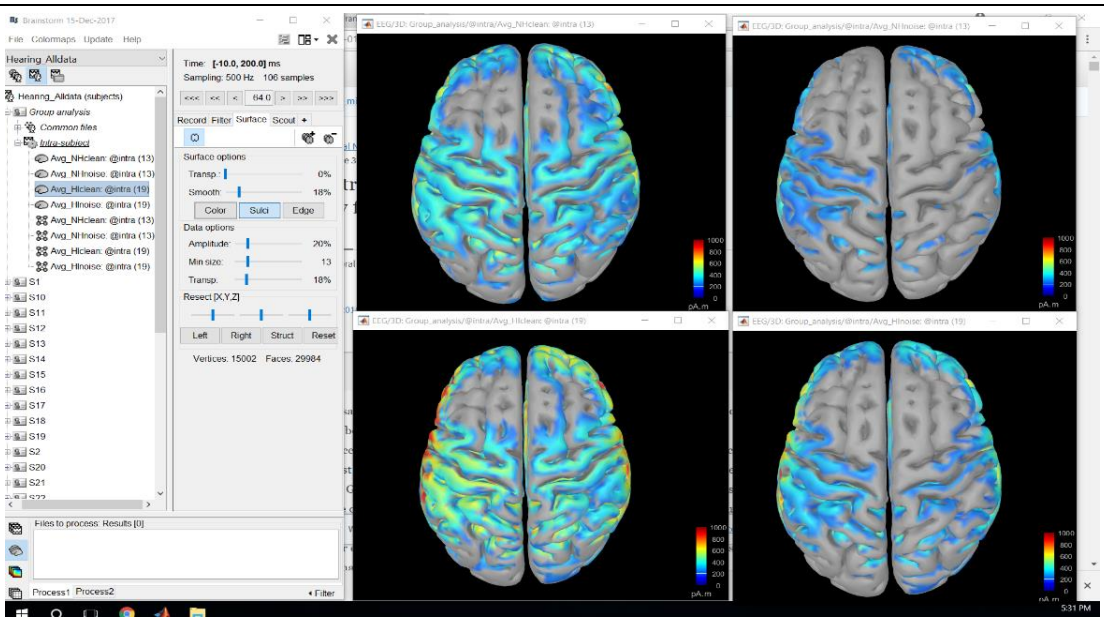

Figure 3.3 Preprocessing in Brainstorm Software

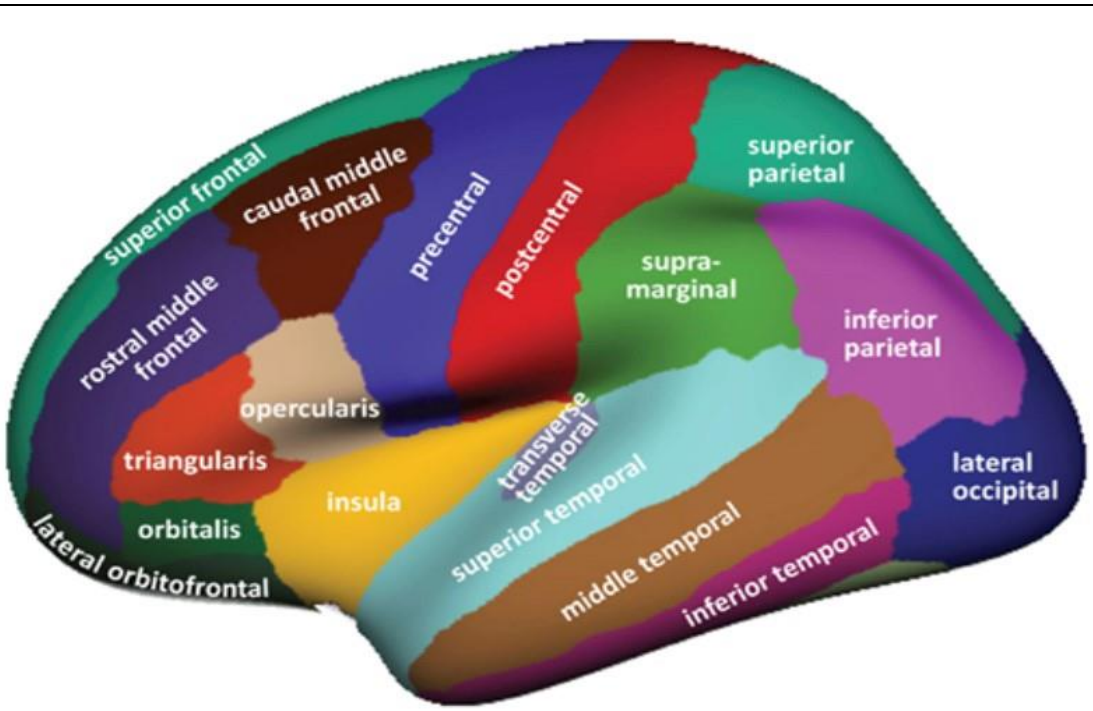

Figure 3.4 Desikan-Killinay Atlas [32]

Table 3.1 Different ROIs Name of Desikan-Killinay Atlas

Shortened Name of DK ROIs	Full DK ROIs' name	Shortened Name of DK ROIs	Full DK ROIs' name
lBKS	bankssts L	lPHIP	parahippocampal L
rBKS	bankssts R	rPHIP	parahippocampal R
lCAC	caudalanteriorcingulate L	lPOP	parsopercularis L
rCAC	caudalanteriorcingulate R	rPOP	parsopercularis R
ICMF	caudalmiddlefrontal L	lPOB	parsorbitalis L
rCMF	caudalmiddlefrontal R	rPOB	parsorbitalis R
lCUN	cuneus L	lPT	parstriangularis L
rCUN	cuneus R	rPT	parstriangularis R
lENT	entorhinal L	lPERI	pericalcarine L
rENT	entorhinal R	rPERI	pericalcarine R
lFP	frontalpole L	lPOC	postcentral L
rFP	frontalpole R	rPOC	postcentral R
lFUS	fusiform L	lPCG	posteriorcingulate L
rFUS	fusiform R	rPCG	posteriorcingulate R
lIP	inferiorparietal L	lPRC	precentral L
rIP	inferiorparietal R	rPRC	precentral R
lIT	inferiortemporal L	lPREC	precuneus L
rIT	inferiortemporal R	rPREC	precuneus R
lINS	insula L	lRAC	rostralanteriorcingulate L
rINS	insula R	rRAC	rostralanteriorcingulate R
lIST	isthmuscingulate L	lRMF	rostralmiddlefrontal L
rIST	isthmuscingulate R	rRMF	rostralmiddlefrontal R
lLO	lateraloccipital L	ISF	superiorfrontal L
rLO	lateraloccipital R	rSF	superiorfrontal R
lLOF	lateralorbitofrontal L	lSP	superiorparietal L
rLOF	lateralorbitofrontal R	rSP	superiorparietal R
lLIN	lingual L	lST	superiortemporal L
rLIN	lingual R	rST	superiortemporal R
lMOF	medialorbitofrontal L	lSUPRA	supramarginal L
rMOF	medialorbitofrontal R	rSUPRA	supramarginal R
lMT	middletemporal L	lTP	temporalpole L
rMT	middletemporal R	rTP	temporalpole R
lPARA	paracentral L	lTRANS	transversetemporal L
rPARAC	paracentral R	rTRANS	transversetemporal R

4. RESULTS

In this section, we will demonstrate connectivity results obtained through PTE and GC analysis. First of all, we will describe the whole-brain connectivity of different cohorts and conditions. Secondly, we will discuss the connectivity of a few ROIs that are associated with speech and language processing. Finally, we will discuss the significant results obtained from the statistical analysis.

4.1. PHASE TRANSFER ENTROPY (PTE)

Phase Transfer Entropy (PTE) is a more robust mathematical model for connectivity analysis. We applied PTE into the time series data at the default setting of the Brainstorm software [31] and measured the whole-brain connectivity by individual and group in both conditions. These results were expressed in normalized value from -0.5 to 0.5. If the connectivity direction is positive, information flow direction, A→B and for negative, B→A. Our results provided a 68×68 connectivity matrix in every subject per condition. Here we show only the group connectivity in circular maps.

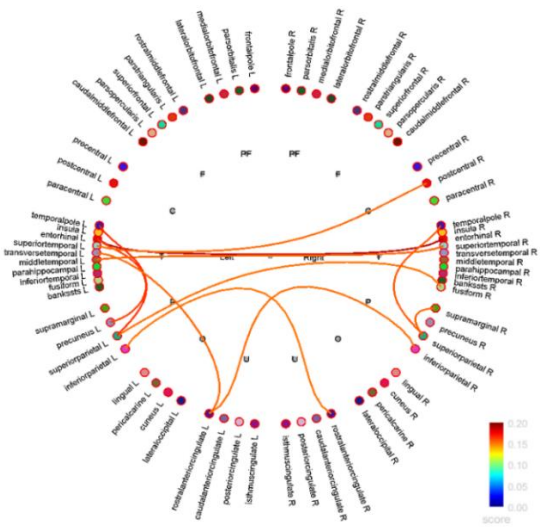

Figure 4.1 PTE connectivity analysis of NH in clean speech perception [2-4 Hz hereafter]

The connectivity links can be found among LH, RH, as well as the intra-hemisphere. Brainstorm has band frequency analysis features; we can visualize the PTE connectivity result in delta (2-4 Hz), theta (5-7 Hz), alpha (8-12 Hz), beta (15-29 Hz) and gamma (30-90 Hz) frequency bands. By default setting of this tool, it chooses delta band frequency, a connectivity distance length of 20 mm, and top 20 % of the connectivity strength. This connectivity result at default setting is depicted in circular connectivity graphs. The connectivity of NH in clean speech detection is presented in Figure-4.1. In this figure, we saw that NH listeners, in clean speech detection, have strong connectivity links found in temporalpole L-> precuneus L, entorhinal L-> entorhinal R. It is remarkable that rostralanteriorcingulate L is weakly connected in both RH and LH of inferiortemporal R, and transversetemporal L. Moreover, the LH has more connection links than the RH. However, if the intensity threshold, frequency band, and connectivity length change the connectivity will also change. For the sake of simplicity, we have chosen the default value for all the analysis.

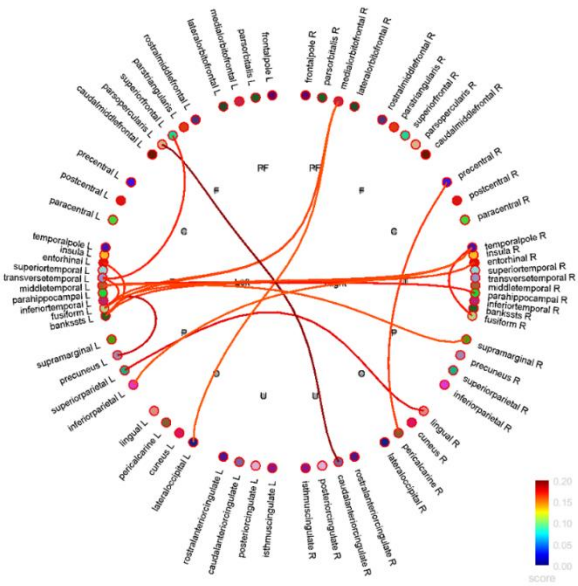

Figure 4.2 PTE connectivity analysis of NL in clean speech perception

The circular connectivity graph of HL listeners in clean speech perception is delineated in Figure 4.2. The strongest connectivity links were found between parsopercularis L and caudalanteriorcingulate R. The precuneus L connected with bankssts L, and precentral R linked with pericalcarine R. Moreover, the temporalpole R is connected with the fusiform R and middletemporal L. Furthermore, transversetemporal L is connected with the fusiform R and superiorfrontal L. From those connectivity results, we found that most of the connectivity was associated with the auditory and language processing regions and few of them are from non-language processing regions.

From circular connectivity maps, we found that the connectivity of NH and HL listeners for clean speech recognition differs from each other.

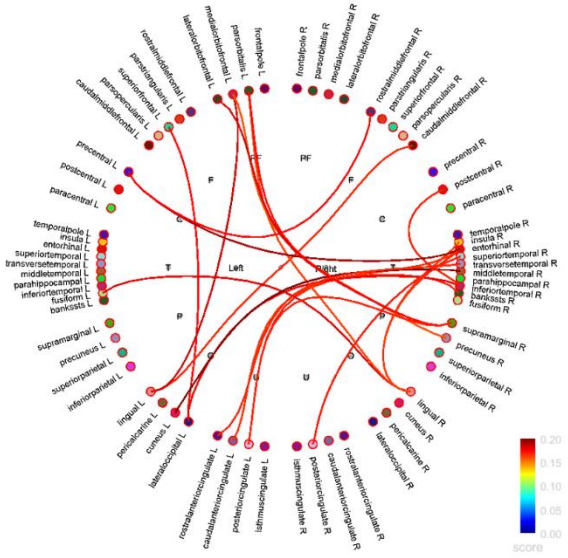

Figure 4.3 PTE connectivity analysis of NH in noise speech perception

For the noisy speech perception, the connectivity maps of NH and HL listeners are shown in Figure 4.3 and Figure 4.4, respectively. The most active connection of NH was found in

precuneus L and entorhinal R, and middletemporal R and cuneus L. Figure 4.3 showed that too many brain regions are interconnected. However, the HL listeners parsopercularis L-> caudalanteriorcingulate L, postcentral R-> fusiform L are strongly connected and parstriangularis L-> posteriorcingulate L are weakly connected and lingual R are interconnected with superiorparietal L, superiorparietal R and entorhinal R.

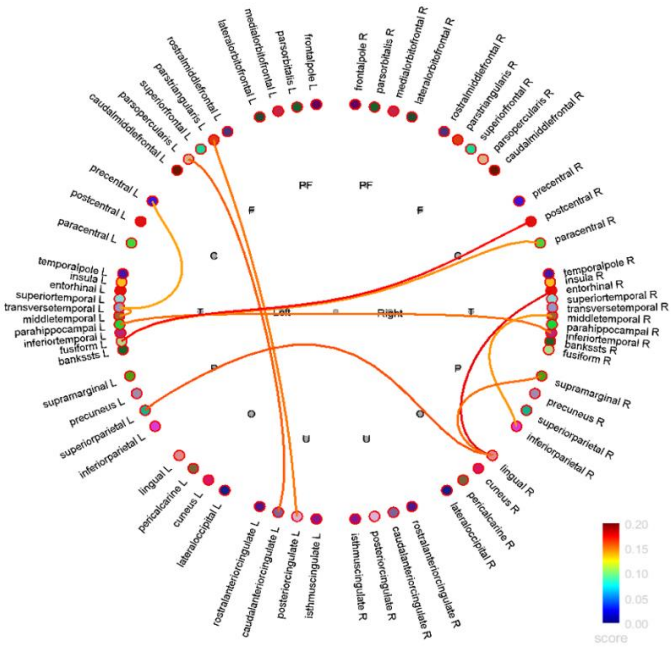

Figure 4.4 PTE connectivity analysis of HL in noise speech perception

To sum up, the connectivity links of NH listeners are less in clean speech recognition, whereas HL listeners have higher connectivity links. On the other hand, in noisy speech perception, NH has more connectivity links than the HL. Within the group, for NH listeners have more connectivities in noisy speech detectiom than clean speech detection. However, HL listeners' connectivities patterns were opposite. From these circular graph connectivity maps, we could not conclude the result precisely.

4.2. GRANGER CAUSALITY (GC)

In this study, we also applied Granger Causality (GC) mathematical approach on the same data and same way for analyzing whole-brain connectivity. The GC is also directional connectivity. Here we only presented the absolute connectivity graph. We considered default setting parameters of the brainstorm software, where the autoregressive order was set to 10. The GC connectivity of NH for clean speech perception is presented in Figure 4.5. Here only two links were found in fusiform R -> caudalanteriorcingulate L, supramarginal L -> supramarginal R. The circular map of connectivity HL in clean speech recognition is depicted in Figure 4.6. Only a link was found between transversetemporal L and middletemporal R.

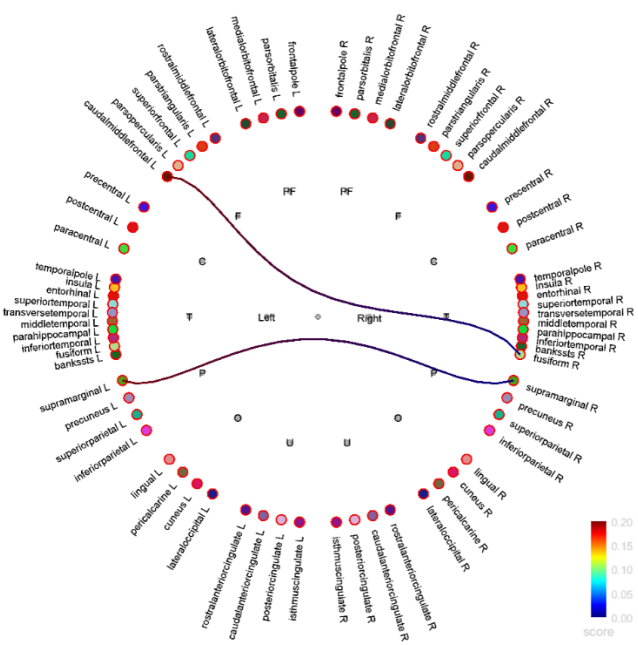

Figure 4.5 GC connectivity analysis of NH in clean speech perception

In the default setting, the connectivity was shown with link a distance at 20 mm and no frequency band option. If we change the threshold strength of the connectivity panel, the connectivity graph also changes. We can find the different connectivity maps by tuning the threshold intensity, and connectivity link distance.

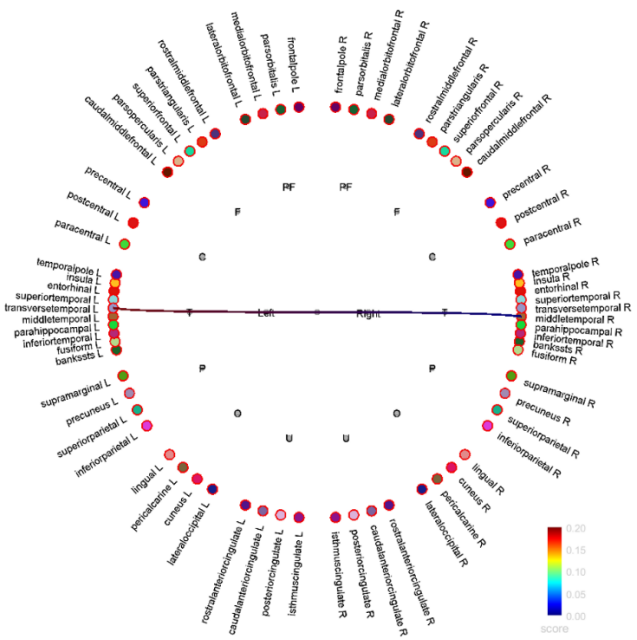

Figure 4.6 GC connectivity analysis of HL in clean speech perception

The default setting connectivity analysis in noisy speech perception of NH and HL listeners is shown in Figure 4.7 and Figure 4.8. The connectivity of NH listeners was found only between inferiortemporal L and fusiform R. However, HL listeners have more connectivity links. The transversetemporal R is connected with the itra-hemisphere region of superiorparietal R. It is noticeable that the RH has more connectivity links than the LH. The middletemporal R was connected with intra-hemisphere parsorbitalis R and inter-hemisphere transversetemporal L and bankssts L.

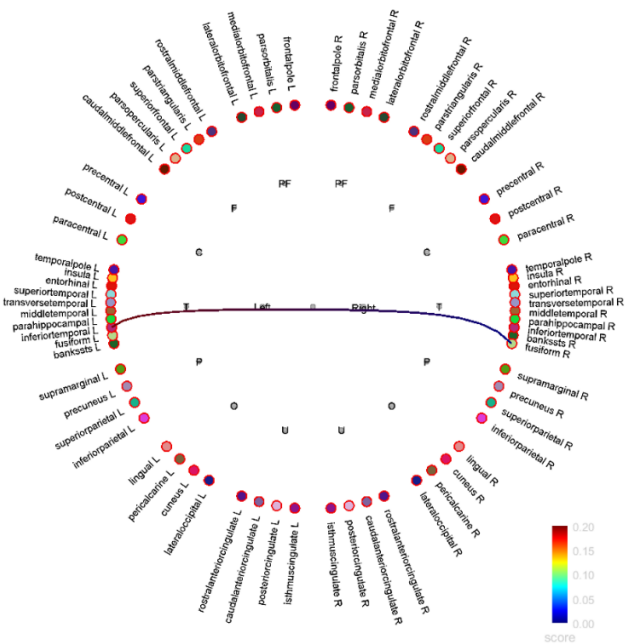

Figure 4.7 GC connectivity analysis of NH in noise speech perception

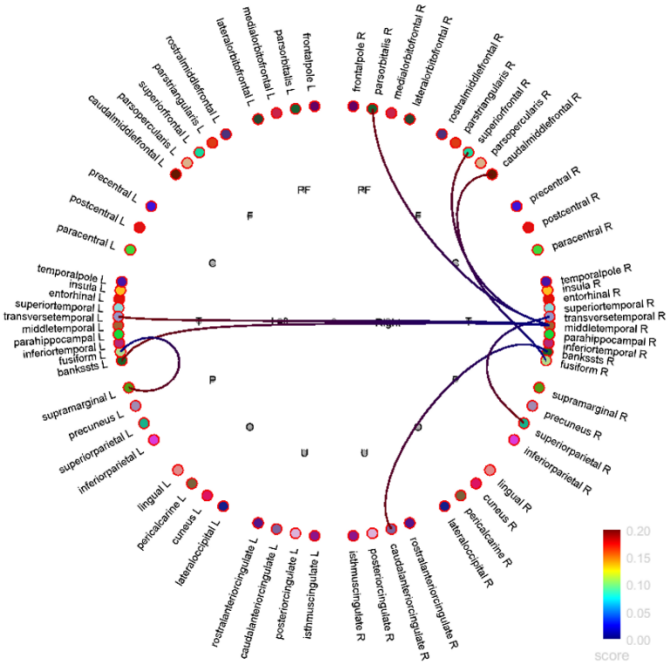

Figure 4.8 GC connectivity analysis of HL in noise speech perception

To sum up, we could not find any threshold selection method or algorithm for the best connectivity analysis in both connectivity (PTE, GC) approaches. So, it is hard to describe the connectivity precisely, or what brain regions are significantly associated with hearing loss and how they were changed. To investigate the significant connectivity change, we have chosen eight ROIs and performed a statistical test by cohort and conditions. The statistical results are described in the next section.

4.3. STATISTICAL ANALYSIS

We have selected 8 ROIs that are associated with auditory and language processing, and performed the statistical test. From this statistical analysis, we figure out differences in connectivity strength. The pairwise connectivity measure in Auditory-Broca's, Auditory-Motor and Broca's-Motor regions are given in Table 4.1.

Table 4.1 ROIs connectivity pairs

Auditory – Broca's area	Broca's- Motor area	Auditory- Motor area
lTRANS-lPT	lPOP - lPRC	lTRANS -lPRC
lTRANS-lPOP	rPOP - rPRC	rTRANS -rPRC
rTRANS-lPT	lPT-lPRC	
rTRANS-rPT	rPT-rPRC	

First of all, we have extracted individual listeners' ROIs' PTE connectivity strength from the whole brain connectivity matrix (i.e., 1-40 Hz). Then from the cohort data, we computed the mean, standard error (SE), and p-values. The p-value was measured from the two samples t-test between NH and HL listeners' in clean and noisy speech perception. The mean, SE, and significant p-value of those ROIs are represented in bar charts. The cohorts' statistical results of Auditory-Broca's areas are shown in Figures 4.9 and 4.10 for clean and noisy speech perception, respectively. In both scenarios, the connectivity patterns of NH and HL listeners are in opposite directions in lTRANS-lPT, lTRANS-lPOP, rTRANS-lPT but the same direction in rTRANS-rPT. In clean speech perception, the mean strength of PTE connectivity at lTRANS-lPT of NH

and HL is 0.02 and -0.10, and SE is 0.05, 0.03 respectively. The lTRANS-lPOP mean strength is almost the same as lTRANS-lPT but a little less in HL. Moreover, in lTRANS-lPOP, the mean of PTE connectivity and SE is 0.02, 0.06 for NH and HL is -0.08 and 0.05. On the other hand, in rTRANS-rPT both NH and HL PTE is negative direction and mean and SE of NH are -0.05, 0.08 and HL are -0.09, 0.04. We found significant p-value only in the LH at lTRANS-lPT and shown with *p in Figure 4.9.

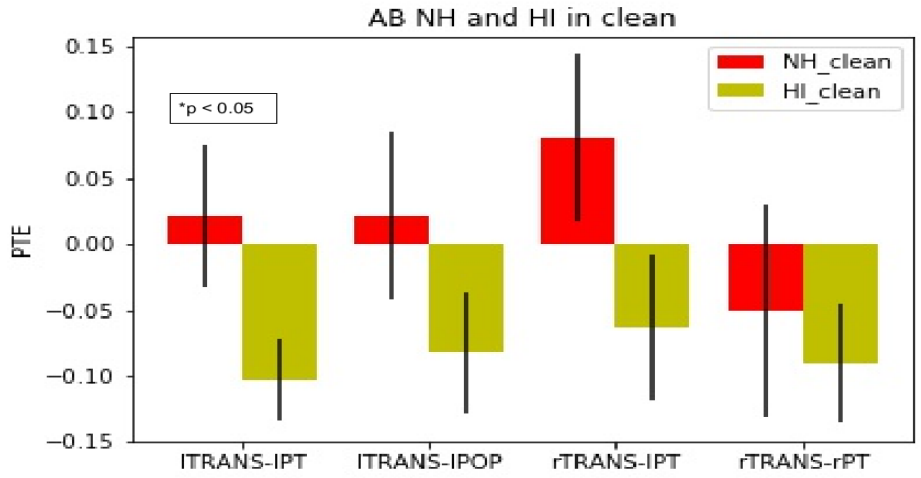

Figure 4.9 PTE statistical analysis in Auditory-Broca's areas in clean speech perception [1-40 Hz hereafter]

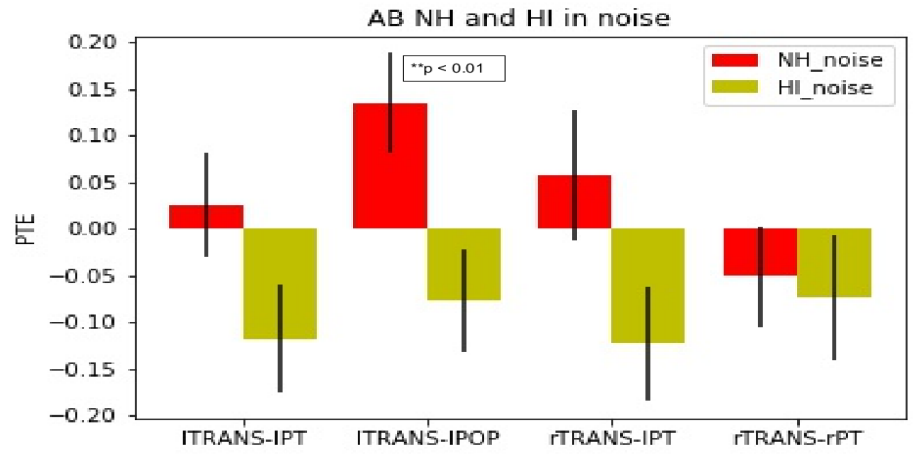

Figure 4.10 PTE statistical analysis in Auditory-Broca's areas in noisy speech perception

In noisy sound perception, the connectivity is measured in Auditory-Broca's regions are almost the same as the clean condition except a significant change was found in lTRANS-lPOP. In this region, the mean connectivity strength and SE are 0.13 and 0.05 for NH and -0.07 and 0.05 for HL. The significant changes were found only in lTRANS-lPOP regions. The p-value is less than 0.01 as shown in figure 4.10 with a **p.

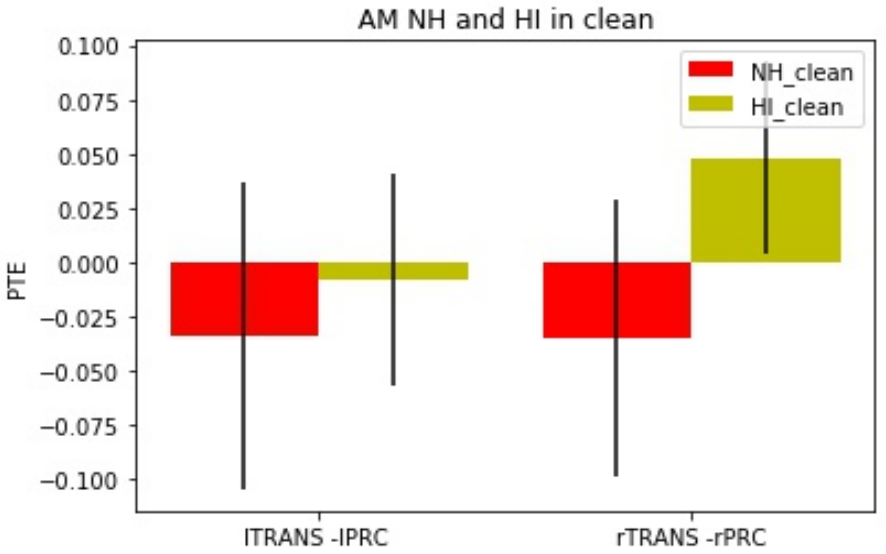

Figure 4.11 PTE statistical analysis in Auditory-Motor areas in clean speech perception

The statistical analysis of Auditory-Motor area for clean and noisy speech recognition is represented in Figure 4.11 and Figure 4.12, respectively. For clean speech detection, a large change was found between the mean PTE strength of NH and HL listeners in lTRANS–lPRC in Auditory-Motor area of LH. The mean PTE connectivity strength and SE of NH is -0.033 and 0.070, and HL is -0.008 and 0.049. However, the mean PTE connectivity in rTRANS–rPRC of RH is in the opposite direction of NH and HL listeners. The mean PTE strength of NH and HL is -0.035 and 0.0482, and SE is 0.064 and 0.044. Though the difference in the LH of Auditory-Motor is substantial, but none of these regions are significant. In noisy sound perception, rTRANS–rPRC region of RH, the mean, and SE of NH and HL listeners are almost same, but in

LH there is a big difference of the mean PTE connectivity strength of NH and HL. The mean strength of HL listeners is fivefold higher than the NH listeners, but this result failed to show significant level p-value.

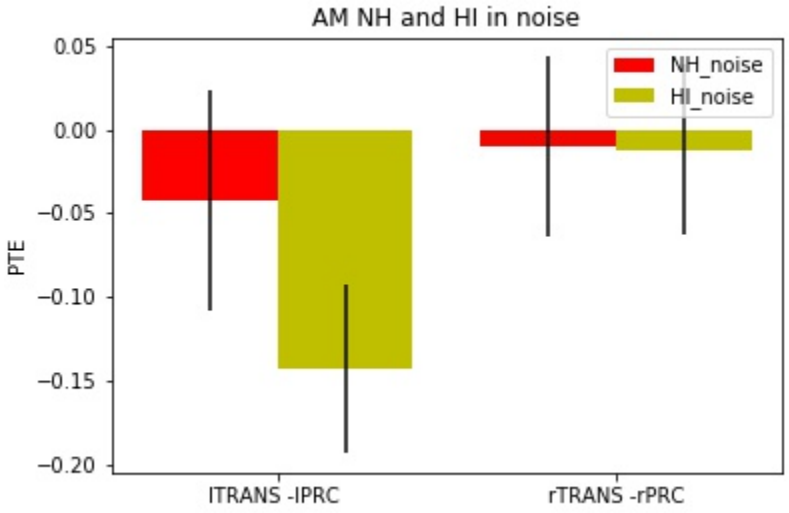

Figure 4.12 PTE statistical analysis in Auditory-Motor areas in noisy speech perception

Now we demonstrate the statistical results of Broca's-Motor areas those obtained from PTE connectivity matrix. The mean and SE of Broca's-Motor area is presented in a bar chart with an error bar. There are four pairwise ROIs. The results of NH and HL listeners for clean speech and noisy speech perception are shown in Figure 4.13 and Figure 4.14, respectively. In clean speech perception, HL listeners mean PTE strength of all the Broca's-Motor area are positive, but NH listeners are negative in the lPOP–lPRC, lPT-lPRC regions. There was a big difference found between NH and HL at lPT-lPRC and lPOP–lPRC, but they are not statistically significant. For noisy speech perception, the connectivity pattern of the NH and HL listeners' connectivity changes more than clean speech detection except the rPOP–rPRC. It is remarkable that the LH and RH connectivity is in the opposite direction at lPOP–lPRC and rPT-rPRC. We have not seen any significant p-value during the t-test.

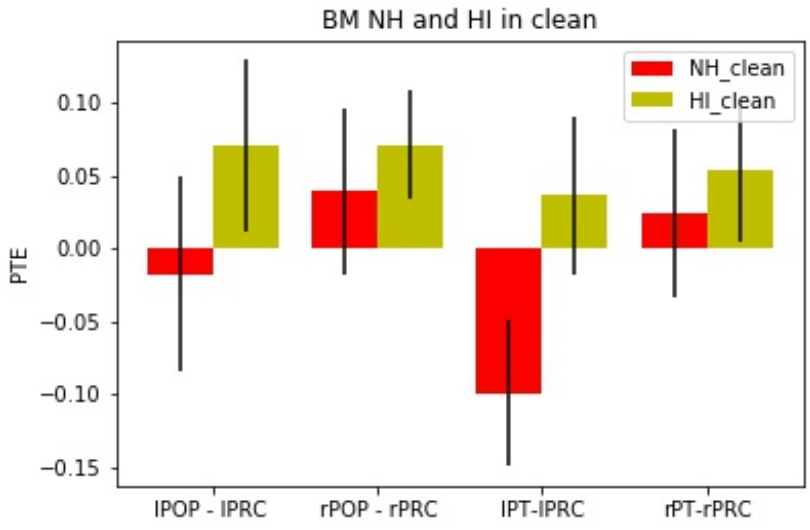

Figure 4.13 PTE statistical analysis in Broca's-Motor areas in clean speech perception

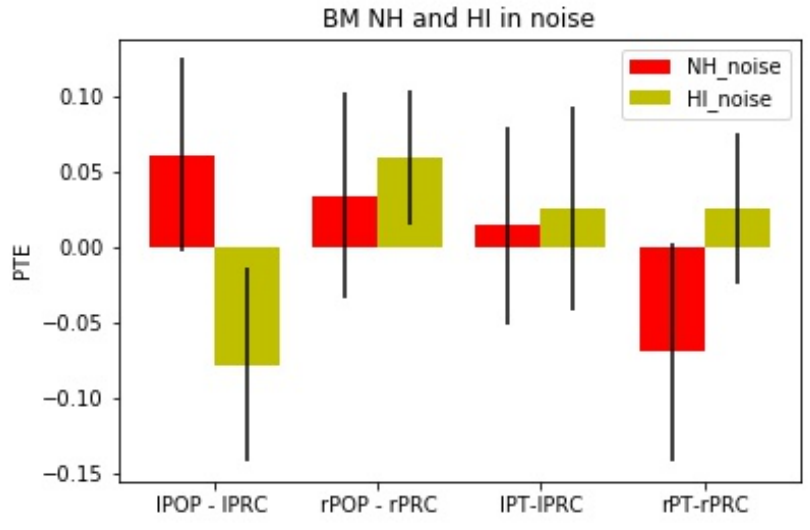

Figure 4.14 PTE statistical analysis in Broca's-Motor areas in noisy speech perception

Here we are going to investigate the GC statistical analysis in Auditory-Broca's, Auditor-Motor, and Broca's-Motor areas. GC is a directed connectivity analysis approach. Because of some limitation of our tools we could only measure the absolute connectivity GC strength.

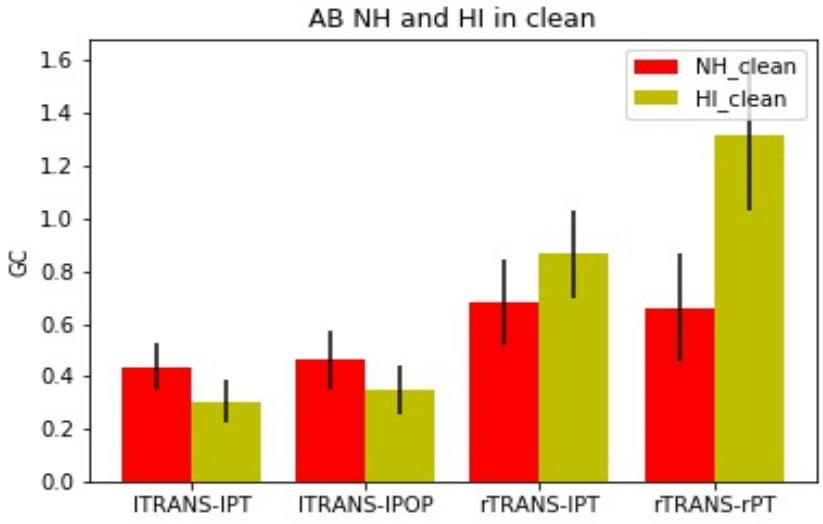

Figure 4.15 GC statistical analysis in Auditory-Broca's areas in clean speech perception

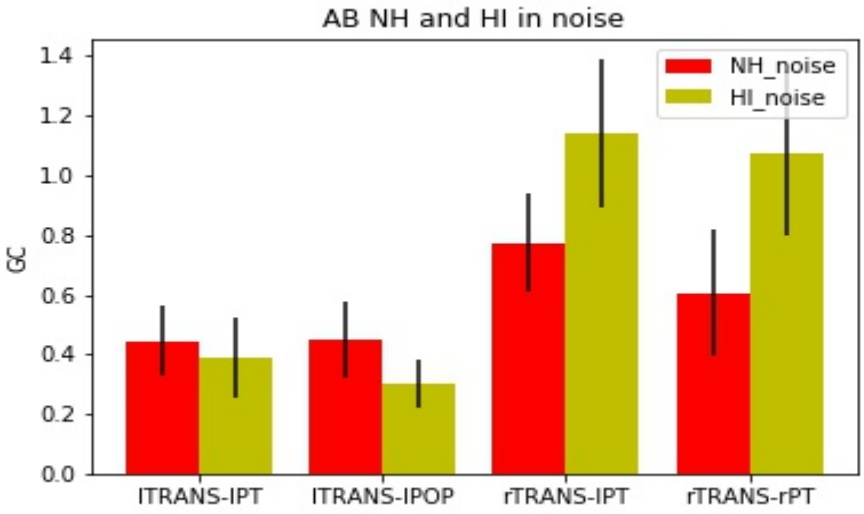

Figure 4.16 GC statistical analysis in Auditory-Broca's areas in noisy speech perception

We extracted the GC connectivity strength from our ROIs by the same procedure of PTE analysis. These results are demonstrated in bar plots with error bars (mean, SE) and p-value if

found within the significant level. The Auditory-Broca's areas of NH and HL listeners for clean and noisy speech perception are depicted in Figure 4.15 and Figure 4.16, respectively. In both conditions, clean and noisy speech recognition, the LH has low GC strength in lTRANS-lPT, lTRANS-lPOP regions of both cohort listeners. It is also noticeable that HL listener GC connectivity strength is a little less than the NH. However, in RH, HL listeners GC mean strength is higher than the NH in lTRANS-lPOP and lTRANS-lPOP areas. None of those regions showed significant p-value.

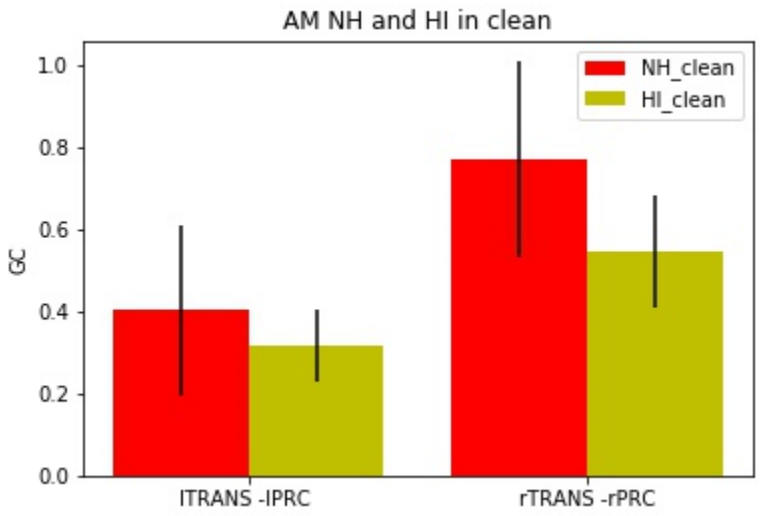

Figure 4.17 GC statistical analysis in Auditory-Motor areas in clean speech perception

The statistical results of Auditory-Motor areas of NH and HL listeners for clean and noisy sound perception are represented in Figure 4.17 and Figure 4.18, respectively. In LH, NH and HL connectivity patterns are the same. On the other hand, in RH, the noisy speech detection the HL listeners' connectivity is stronger than the NH. In clean speech detection, the mean and SE of GC strength at rTRANS-rPRC is 0.768 and 0.239 for NH and 0.544 and 0.133 for HL but in noisy speech detection, these are 0.447 and 0.119 for NH and 0.638 and 0.146 for HL. This

stronger connectivity in noisy condition indicates that RH is associated with noisy speech perception in HL listeners.

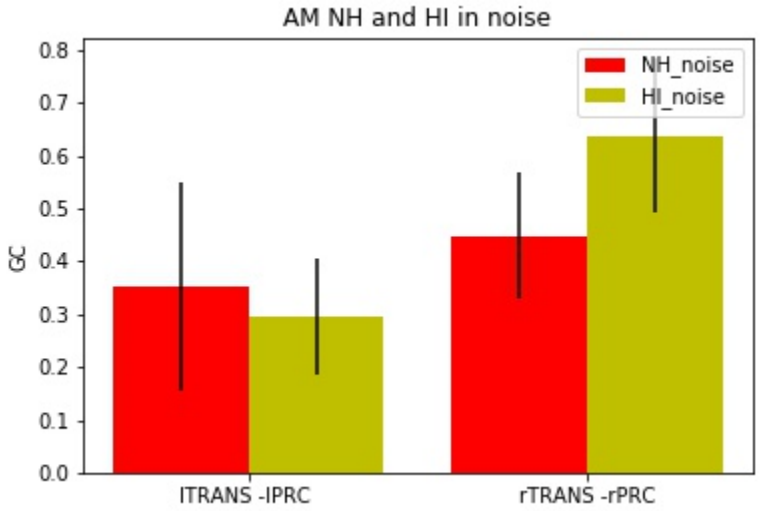

Figure 4.18 GC statistical analysis in Auditory-Motor areas in noisy speech perception

The GC statistical analysis of Broca's-motor areas is presented in Figure 4.19 and Figure 4.20 for clean and noisy speech recognition. In clean speech detection, there is a big difference between NH and HL listeners found in lPOP–lPRC and lPT-lPRC regions of LH. The GC mean and SE at lPOP–lPRC are 0.569 and 0.137 for NH, 0.236 and 0.046 for HL, respectively. Moreover, in the lPT-lPRC region mean and SE of NH is 0.622 and 0.213, and HL is 0.254 and 0.078. Though there is a big difference between NH and HL listener, in the LH of those regions, the only statistically significant p-value was found in lPOP–lPRC.

In noisy sound detection, the HL has strong connectivity than NH in RH. The GC mean strength and SE in rPOP–rPRC of NH are 0.354 and 0.086, for HL are 0.390 and 0.091, in rPT-rPRC region NH mean and SE are 0.190 and 0.062 and HL are 0.311 and 0.0781.

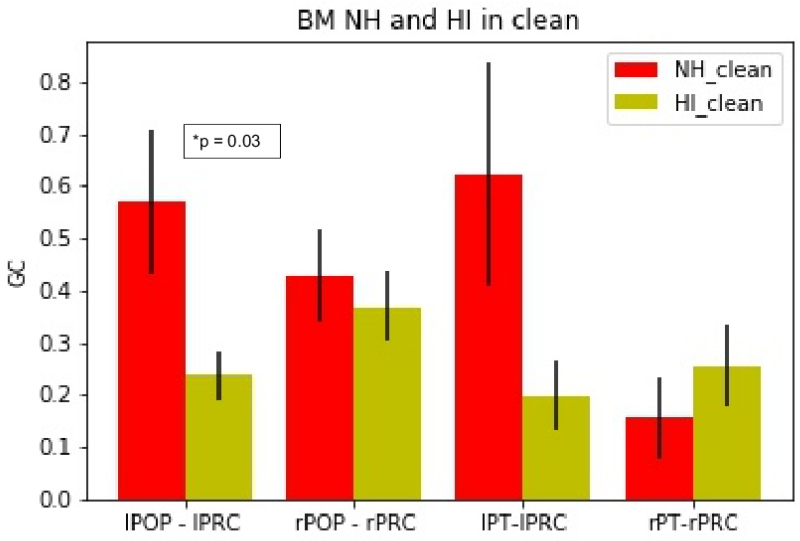

Figure 4.19 GC statistical analysis in Broca's-Motor areas in clean speech perception

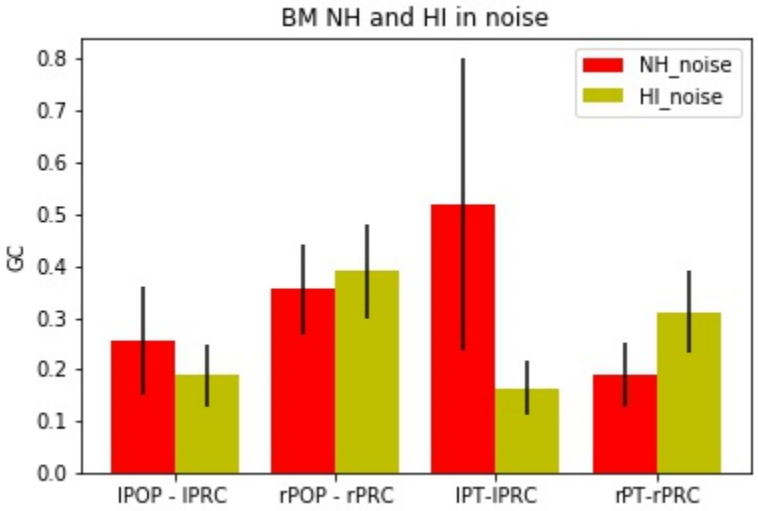

Figure 4.20 GC statistical analysis in Broca's-Motor areas in noisy speech perception

In summary, so far we discussed the connectivity maps and statistical analysis (mean, SE, and p-value). We found the only significant p-value in the LH of Auditory-Broca's area in clean as well as the noisy speech perception in case of PTE connectivity analysis. On the other hand,

when we applied the GC connectivity analysis, we found significant p-value in the Broca's-Motor area in the LH. However, there is no statistically significant result in noisy speech perception. This was reflected in the literature reviewed that GC is not suitable for noisy signal analysis.

4.4. OVERALL CONNECTIVITY COMPARISION

In this section, we will discuss how the NH and HL listeners' connectivity changes in the auditory-language processing regions, in the point of view of top-down and bottom-up mechanisms.

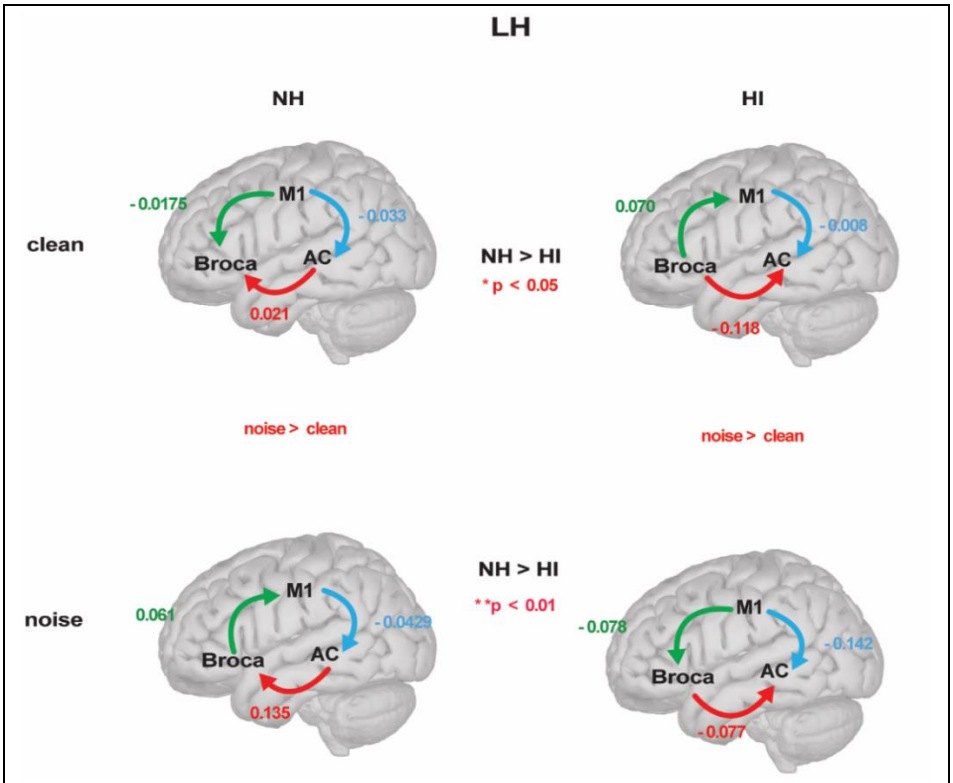

Figure 4.21 PTE connectivity analysis with a significant p-value

The overall auditory and language processing connectivity analysis was obtained from the PTE analysis and demonstrated in Figure 4.21. In clean speech perception, NH listeners communicate with a bottom-up technique, but HL listeners communicate in a top-down method. In Auditory-Broca's region, NH listeners communicate in a bottom-up manner, but HL listeners

communicate in a top-down manner. The lTRANS-lPT of the Auditory-Broca's area is statistically significant, and $p < 0.05$. Moreover, NH listeners also communicate in a bottom-up way in Motor to Broca's area. However, the HL listeners communicate with a top-down approach. Interestingly, the Motor to Auditory communication pathway was the same in both NH and HL listeners.

In the case of noisy speech detection, the NH listeners' communication direction is Broca's area to Motor area but HL listeners communication is the opposite (e.g., Motor to Broca's area). Auditory to Broca communication is a bottom-up way (e.g., Auditory to Broca's area) but HL listeners' communication in the opposite way (Broca's area to Auditory area). The Auditory-Broca's region (lTRANS-lPOP) of LH is statistically significant $p < 0.01$. The Motor to Auditory communication direction remains the same in NH and HL and also in clean and noisy speech perception. In clean speech detection, we found the significant level change in the lTRANS-lPT of Auditory-Broca's area and for noisy sound detection, significant change was in the (lTRANS-lPOP), but both pairs are in the Auditory-Broca's area of LH. Because of spatial error, our results showed nearest two regions, but both regions within the Auditory–Broca's of LH and they are very close to each other.

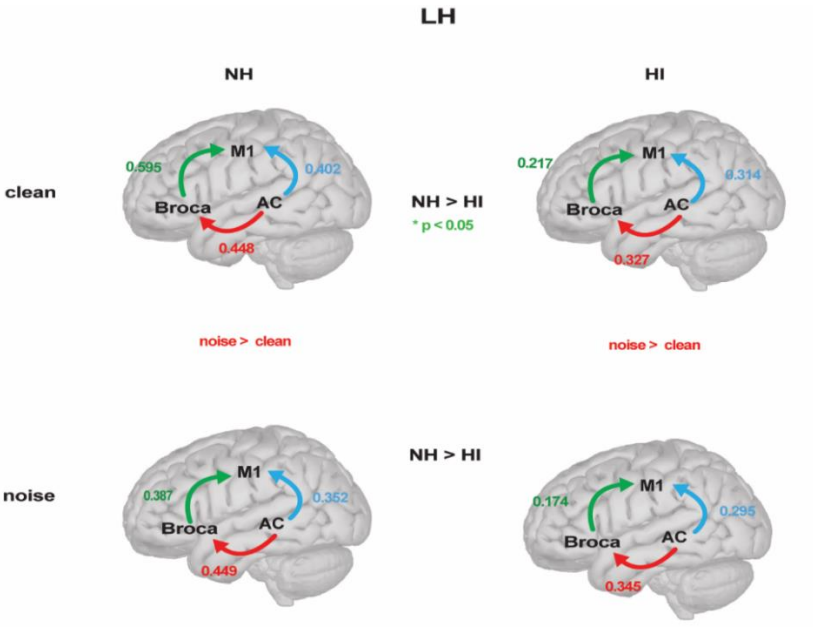

Figure 4.22 GC connectivity analysis with a significant p-value

The summary of GC connectivity analysis is shown in Figure 4.22. Here we have an only absolute GC connectivity strength. So we will discuss only the connectivity strength not the direction. For simplicity of representation, we showed that all the regions information flow in same way. In case of clean sound recognition, the Auditory-Broca's area signal strength of NH is higher than the HL listeners. Broca's-Motor area connectivity strength of NH is double of HL listeners. Furthermore, Auditory-Motor area connectivity of NH is higher than the HL listeners. We found the significant $p < 0.03$ value only in the Broca's-Motor area while compared NH and HL listeners. So, this is the only pair of regions that differs between groups. On the other hand, in noisy sound perception, the connectivity strength of NH in Auditory-Broca's, Broca's-Motor and Auditory-Motor area are higher than the HL listeners. None of those regions exhibit significant statistical results.

4.5. NEURAL AND BEHAVIORAL CORRELATION

To investigate the neural and behavioral correlation, we used the Generalized Linear Mixed Effects (GLME) logistic regression model. This model is used for binary outcome variable modeling. The logistic regression model allows us to find the relationship between binary outcome variables and a group of predictor variables. Let's say if z is the binary outcome variable either success or failure *(i.e.,* 1/0), p is the success probability of z, and y_1, y_2,…. y_n are a set of predictor variables. The logistic regression of z on y_1 , y_2,…. y_n can estimate the parameter values α_1, α_2……α_n via the maximum likelihood threshold [34] . The logistic regression expression is:

$$logit(p) = log\left(\frac{p}{1-p}\right) = \alpha_0 + \alpha_1 y_1 + \cdots \ldots \alpha_n * y_n$$

Here, we have predicted the speech perception accuracy (0-100%) from the above expression by taking the input parameters PTE, PTA, cohort, and stimulus. The GLME logistic regression model showed for NH listeners, a one-unit change of PTE, and the odds speech detection accuracy is ~9 at a p-value7.7×10^{-7}. However, for HL listeners a one-unit change of PTE, odds speech detection accuracy is ~2 and significant p-value 0.003. It is observed that HL listeners' performance was lower than the NH listeners (Figure 3.2B). Moreover, the noisy speech degrades the behavioral accuracy in both groups. Both NH and HL listeners' performance degraded in noisy speech detection.

5. CONCLUSION

In this thesis, we localized the source of EEG data from scalp surface potentials. Furthermore, we extracted time series data from the cortical surface and investigated the whole brain connectivity through the Granger Causality and Phase Transfer Entropy. We also performed the statistical analysis in auditory-linguistic processing areas of the brain and found that connectivity between primary auditory cortex and Broca's area differs among age-matched NH and HL listeners. Auditory-Broca's area results are significant. For clean speech detection, p-value is <0.03. For noisy speech detection, p-value is <0.01. The GLME results revealed that HL group speech detection performance was lower than that of the NH group and was related to changes in auditory-linguistic brain connectivity. These results imply that neural results were reflected in the behavioral results.

Limitation of our work: We investigated the connectivity analysis for only 200 ms. For source localization, we used sLORETA with BEM that has maximum error ~ 20 mm [10]. Moreover, for GC analysis, we considered an autoregressive (AR) order of 10 and could not find the phase information. We got many null results in PTE/ GC connectivity analysis because of source localization error. We tried to find the adaptive threshold for circular maps connectivity representation by using interquartile range, local adaptive threshold, mean and median. Unfortunately, none of them provide better results for our data. We represented the circular maps only for top 20 % connectivity strength.

6. REFERENCES

[1] F. R. Lin *et al.*, "Hearing loss and cognitive decline in older adults," *JAMA Intern. Med.*, vol. 173, no. 4, pp. 293–299, 2013.

[2] G. M. Bidelman and A. Yellamsetty, "Noise and pitch interact during the cortical segregation of concurrent speech," *Hear. Res.*, vol. 351, pp. 34–44, 2017.

[3] K. E. Bainbridge and M. I. Wallhagen, "Hearing loss in an aging American population: extent, impact, and management," *Annu. Rev. Public Health*, vol. 35, pp. 139–152, 2014.

[4] C. J. Murray *et al.*, "The state of US health, 1990-2010: burden of diseases, injuries, and risk factors," *Jama*, vol. 310, no. 6, pp. 591–606, 2013.

[5] F. Babiloni *et al.*, "Estimation of the cortical functional connectivity with the multimodal integration of high-resolution EEG and fMRI data by directed transfer function," *Neuroimage*, vol. 24, no. 1, pp. 118–131, 2005.

[6] G. F. Woodman, "A brief introduction to the use of event-related potentials in studies of perception and attention," *Atten. Percept. Psychophys.*, vol. 72, no. 8, pp. 2031–2046, 2010.

[7] M. X. Cohen, "Where does EEG come from and what does it mean?," *Trends Neurosci.*, vol. 40, no. 4, pp. 208–218, 2017.

[8] M. Rubinov and O. Sporns, "Complex network measures of brain connectivity: Uses and interpretations," *NeuroImage*, vol. 52, no. 3, pp. 1059–1069, Sep. 2010.

[9] O. Sporns, "Brain connectivity," *Scholarpedia*, vol. 2, no. 10, p. 4695, Oct. 2007.

[10] Z. A. Acar and S. Makeig, "Effects of forward model errors on EEG source localization," *Brain Topogr.*, vol. 26, no. 3, pp. 378–396, 2013.

[11] Z. J. Koles, "Trends in EEG source localization," *Electroencephalogr. Clin. Neurophysiol.*, vol. 106, no. 2, pp. 127–137, Feb. 1998.

[12] C. Plummer, A. S. Harvey, and M. Cook, “EEG source localization in focal epilepsy: Where are we now?,” *Epilepsia*, vol. 49, no. 2, pp. 201–218, Feb. 2008.

[13] J. Song *et al.*, “EEG source localization: sensor density and head surface coverage,” *J. Neurosci. Methods*, vol. 256, pp. 9–21, 2015.

[14] E. Barzegaran and M. G. Knyazeva, “Functional connectivity analysis in EEG source space: The choice of method,” *PloS One*, vol. 12, no. 7, p. e0181105, 2017.

[15] G. Wang and D. Ren, “Effect of brain-to-skull conductivity ratio on EEG source localization accuracy,” *BioMed Res. Int.*, vol. 2013, 2013.

[16] A. M. Bastos and J.-M. Schoffelen, “A tutorial review of functional connectivity analysis methods and their interpretational pitfalls,” *Front. Syst. Neurosci.*, vol. 9, p. 175, 2016.

[17] M. Hassan, O. Dufor, I. Merlet, C. Berrou, and F. Wendling, “EEG source connectivity analysis: from dense array recordings to brain networks,” *PloS One*, vol. 9, no. 8, p. e105041, 2014.

[18] A. K. Seth, A. B. Barrett, and L. Barnett, “Granger causality analysis in neuroscience and neuroimaging,” *J. Neurosci.*, vol. 35, no. 8, pp. 3293–3297, 2015.

[19] M. Lobier, F. Siebenhühner, S. Palva, and J. M. Palva, “Phase transfer entropy: a novel phase-based measure for directed connectivity in networks coupled by oscillatory interactions,” *Neuroimage*, vol. 85, pp. 853–872, 2014.

[20] P. A. Stokes and P. L. Purdon, “A study of problems encountered in Granger causality analysis from a neuroscience perspective,” *Proc. Natl. Acad. Sci.*, vol. 114, no. 34, pp. E7063–E7072, 2017.

[21] A. M. Lesicko and D. A. Llano, “Impact of peripheral hearing loss on top-down auditory processing,” *Hear. Res.*, vol. 343, pp. 4–13, 2017.

[22] L. Shuai and T. Gong, “Temporal relation between top-down and bottom-up processing in lexical tone perception,” *Front. Behav. Neurosci.*, vol. 8, p. 97, 2014.

[23] G. M. Bidelman, C. E. Nelms Price, S. D, S. Arnott, and C. Alain, “Afferent-efferent connectivity between auditory brainstem and cortex accounts for poorer speech-in-noise perception in older adults,” Under reviewed.

[24] G. M. Bidelman, “Towards an optimal paradigm for simultaneously recording cortical and brainstem auditory evoked potentials,” *J. Neurosci. Methods*, vol. 241, pp. 94–100, Feb. 2015.

[25] M. C. Killion, P. A. Niquette, G. I. Gudmundsen, L. J. Revit, and S. Banerjee, “Development of a quick speech-in-noise test for measuring signal-to-noise ratio loss in normal-hearing and hearing-impaired listeners,” *J. Acoust. Soc. Am.*, vol. 116, no. 4, pp. 2395–2405, Oct. 2004.

[26] C. Alain, K. McDonald, and P. Van Roon, “Effects of age and background noise on processing a mistuned harmonic in an otherwise periodic complex sound,” *Hear. Res.*, vol. 283, no. 1, pp. 126–135, Jan. 2012.

[27] G. M. Bidelman and M. Howell, “Functional changes in inter-and intra-hemispheric cortical processing underlying degraded speech perception,” *Neuroimage*, vol. 124, pp. 581–590, 2016.

[28] G. M. Bidelman, “Multichannel recordings of the human brainstem frequency-following response: scalp topography, source generators, and distinctions from the transient ABR,” *Hear. Res.*, vol. 323, pp. 68–80, May 2015.

[29] R. Oostenveld and P. Praamstra, “The five percent electrode system for high-resolution EEG and ERP measurements,” *Clin. Neurophysiol.*, vol. 112, no. 4, pp. 713–719, 2001.

[30] T. W. Picton, P. van Roon, M. L. Armilio, P. Berg, N. Ille, and M. Scherg, “The correction of ocular artifacts: a topographic perspective,” *Clin. Neurophysiol.*, vol. 111, no. 1, pp. 53–65, Jan. 2000.

[31] F. Tadel, S. Baillet, J. C. Mosher, D. Pantazis, and R. M. Leahy, “Brainstorm: a user-friendly application for MEG/EEG analysis,” *Comput. Intell. Neurosci.*, vol. 2011, p. 8, 2011.

[32] R. S. Desikan *et al.*, “An automated labeling system for subdividing the human cerebral cortex on MRI scans into gyral based regions of interest,” *NeuroImage*, vol. 31, no. 3, pp. 968–980, Jul. 2006.

[33] G. L. Wallstrom, R. E. Kass, A. Miller, J. F. Cohn, and N. A. Fox, “Automatic correction of ocular artifacts in the EEG: a comparison of regression-based and component-based methods,” *Int. J. Psychophysiol.*, vol. 53, no. 2, pp. 105–119, Jul. 2004.

[34] J. Bruin, “Newtest: command to compute new test. UCLA:,” Feb. 2011.